UNDERSTANDING THE ERRORS IN CHAMP ACCELEROMETER-DERIVED NEUTRAL MASS DENSITY DATA

Timothy Kodikara*[1], Isabel Fernandez-Gomez[1], Ehsan Forootan[2], W. Kent Tobiska[3], and Claudia Borries[1]

[1]German Aerospace Center, Kalkhorstweg 53, 17235 Neustrelitz, Germany
[2]Geodesy and Earth Observation Group, Department of Planning, Aalborg University, Rendburggade 14, 9000, Denmark
[3]Space Environment Technologies, Pacific Palisades, CA, USA
***correspondence:** timothy.kodikara@dlr.de

Key Points

- Examines errors in CHAMP accelerometer-derived neutral mass density products
- Strong latitude dependence in estimated errors for both data and models
- Assumptions in neutral mass density derivation strongly influence error estimates

ABSTRACT

Accelerometer-derived neutral mass density (NMD) is an important quantity describing the variability of the upper atmosphere. NMD is widely used to calibrate and validate some models used for satellite orbit determination and prediction. Quantifying the true NMD is nearly impossible due to, among others, the lack of simultaneous in-situ measurements for cross-validation and the incomplete characterization of the uncertainties of these NMD products. This study investigates the error distribution of three different accelerometer-derived NMD products from the CHAMP satellite mission during time periods of both high and low solar activity. Using a multimodel ensemble comprised of both physical and empirical models, the study characterizes the error variance of the NMD. The strategies employed here may be useful and applicable to other space missions spanning over longer time periods. The results show considerable differences among the three CHAMP data sets and also reveal a pronounced latitude dependence in their error distributions. The median error standard deviation of CHAMP NMD is smaller during time periods of high solar activity (11.0%) than during periods of low solar activity (13.1%). The results indicate that the method of processing the accelerometer data has a significant impact on the uncertainty estimates of the different CHAMP NMD products.

Plain Language Summary

The accelerometer on board the CHAMP satellite measured the nongravitational acceleration. Using these measurements, several CHAMP in-situ neutral mass density (NMD) products have been published. Such NMD products are useful for furthering our understanding of thermospheric dynamics. NMD is one of the major sources of uncertainty in the tracking and prediction of low-Earth orbit satellites—an essential undertaking in the management and sustainment of space assets. Researchers and satellite operators rely on NMD observations to calibrate and validate the models they use to estimate and forecast NMD. Therefore, incorporating the uncertainties of NMD data during model development and calibration is critical to improve the reliability of forecasts and to accurately assess the risk of satellite collisions. In this study, we use several statistical techniques and models to gain new insights into the CHAMP NMD data. Using a multimodel ensemble, we characterize the error variance of the NMD. Our results show a pronounced latitude dependence for the estimated errors. The results suggest that the method of processing the accelerometer data has a significant impact on the uncertainty estimates of different NMD products. We also show that these estimated errors are generally small during periods of high solar activity.

1 Introduction

Near-Earth space is home to many satellites that are critical to sustaining our modern lifestyles and economies—relying on space-based technologies for services such as communications, navigation, agriculture, security, banking, and healthcare. More than half of these operational satellites are in low Earth orbit region (LEO; 160–2000 km), which is also the region most populated with space debris (European Space Agency, 2021, and references therein). And so the risk of satellite collisions is higher in LEO. Studies (e.g., Emmert et al., 2017; Hejduk and Snow, 2018; Vallado and Finkleman, 2014) show that neutral mass density is one of the most significant sources of uncertainty in LEO orbit tracking and prediction—an essential enterprise in managing and sustaining space assets. Researchers and satellite operators rely on neutral mass density observations to validate the models they use to estimate and forecast neutral mass density.

Accelerometer-derived neutral mass density from some LEO satellites, among others, is one of the most widely used sources to calibrate and validate upper atmosphere models (e.g., Kodikara et al., 2018; Mehta et al., 2017; Morozov et al., 2013; Shim et al., 2012; Sutton, 2018). Thus, incorporating the uncertainties associated with the data during model development and calibration is critical to improve the reliability of the forecasts and to accurately assess the risk of collision with operational satellites. Bussy-Virat et al. (2018) and Hejduk and Snow (2018) point out that most of the upper atmosphere models do not have the capability to provide the uncertainty of the estimated neutral mass density to the user. This is partly due to an incomplete understanding of the uncertainties associated with the input data. For example, Bowman et al. (2008) and Weimer et al. (2016) describe the use of scale factors to correct for modeling errors caused by observations used to calibrate the model. Some recent (e.g., March et al., 2019; Mehta et al., 2017; Tobiska et al., 2021) and ongoing Jackson et al. (2020) work focuses on the accuracy and consistency of thermospheric neutral mass density data sets.

The accelerometer-derived neutral mass density from the CHAMP (CHAllenging Minisatellite Payload) mission, which contributed to significantly advance our understanding of the upper atmosphere through its simultaneous observations of plasma, neutrals, and the magnetic field Stolle and Liu (2014), is the focus of this study. The accelerometers measure the nongravitational acceleration on-board, which provides a direct means of calculating the atmospheric drag acting on a spacecraft under certain assumptions Emmert (2015). King-Hele and Scott (1970) describe that neutral mass density can be derived from orbital decay information as a function of mean angular motion, altitude change, drag acceleration, and several other known parameters and estimates specific to the spacecraft. The expression for the neutral mass density (ρ) imparted atmospheric drag acceleration a_{drag} is as follows:

$$a_{drag} = -\left(\frac{C_d S_{area}}{S_{mass}}\right)\frac{1}{2}\rho V_{rel}^2, \quad (1)$$

where C_d is the atmospheric drag coefficient, V_{rel} is the velocity of the satellite relative to the atmosphere, S_{area} is the cross-sectional area of the satellite normal to V_{rel}, and S_{mass} is the mass of the satellite. The atmospheric drag causes the satellite to slow down, as indicated by the negative sign, and to lose altitude. While the term $C_d S_{area}/S_{mass}$, which is also known as the ballistic coefficient, does not vary much over the lifetime of the satellite, the dynamic pressure on the satellite $\rho V_{rel}^2/2$ decreases rapidly with increasing altitude. Although CHAMP's STAR (spatial triaxial accelerometer for research) accelerometer has a relatively high resolution (Bruinsma et al. (2004)), it is difficult to obtain absolute nongravitational acceleration as close as possible. This is due to the difficulty of replicating the operational environment in space to calibrate the accelerometer in a laboratory prior to launch. Bruinsma et al. (2004) summarize the iterative procedure used to calibrate the CHAMP accelerometer from measurements taken in orbit.

The uncertainties in accelerometer-derived CHAMP neutral mass densities originate from many sources, such as the errors in the nongravitational model and the calibration of the accelerometer (e.g., Bruinsma et al., 2004; Doornbos, 2012; Sutton et al., 2007). Accelerometer calibration methods, scaling factors, background models, and assumptions about the exact source of acceleration and neutral wind speed contribute to these uncertainties. Quantifying the true neutral mass density of these historical data sets is nearly impossible due to, among others, the lack of simultaneous in-situ measurements to cross-validate, and the incomplete characterization of these uncertainties that propagate into the derived neutral mass density product. The different methods of extracting neutral mass density from accelerometer measurements cause the differences between the data sets (e.g., Mehta et al., 2017; March et al., 2019), and their uncertainties are not fully understood.

In this study, we examine three different accelerometer-derived neutral mass density products from CHAMP: Mehta et al. (2017) (PM), Sutton (2011) (ES), and Doornbos (2012) (TU). We use several different statistical techniques, physical and empirical models, and the newly released Tobiska et al. (2021) HASDM (high accuracy satellite drag model) data set to gain new insights into these CHAMP data products. We present the error estimates of the neutral mass density products by applying the Grubbs (1948)' method to a multimodel ensemble consisting of both physical and empirical models of the upper atmosphere. Section 2 describes the models used in this study. Section 3 reviews the above-mentioned strategies in detail. Section 4 describes the main results of the work. Section 5 discusses the results and limitations of the work, and section 6 summarizes the conclusions of the study.

2 Models

2.1 TIE-GCM

TIE-GCM (thermosphere-ionosphere-electrodynamics general circulation model) is a three-dimensional, time-

dependent, physics-based model of the thermosphere and ionosphere Richmond et al. (1992). The website <www.hao.ucar.edu/modeling/tgcm> hosts the open-source TIE-GCM code. See Kodikara (2019) and Qian et al. (2014) for summaries of recent developments in the model. In this study, we use TIE-GCM version 2.0 (released on 21 March 2016) with a horizontal resolution of 2.5°×2.5° in geographic latitude and longitude, and a vertical resolution of 0.25 scale-height. We specify the solar irradiance input to the model via an empirical solar proxy model—the extreme ultraviolet flux model for aeronomic calculations (EUVAC; Richards et al. (1994); Solomon and Qian (2005)). This empirical formulation uses the average of the daily solar flux $F_{10.7}$ and its 81-day centered mean $\overline{F}_{10.7}$. Here, we use the value observed by the ground-based solar radio telescope, as it is more suitable for upper-atmospheric applications than the $F_{10.7}$ adjusted for Earth-Sun distance Tapping (2013). We use the Kp index-based Heelis et al. (1982) ion convection model, and the Roble and Ridley (1987) auroral particle precipitation scheme (with modifications from Emery et al. (2012)) to specify the magnetospheric forcing that describes the high-latitude mean energy, energy flux, and electric potential. To account for the tidal forcing from the lower atmosphere, we use the Hagan et al. (2001) global scale wave model (GSWM) to perturb the lower boundary of TIE-GCM. Here, the GSWM specifies the migrating-diurnal and -semidiurnal tides, which add perturbations to the zonal mean neutral temperature and horizontal winds, among others. We also add perturbations to the advective and diffusive transport via the eddy-diffusion-coefficient described in Qian et al. (2009). Herein, a model run configured in this way refers to a standalone or geophysical indices (GPI)-driven TIE-GCM.

2.2 Mass Spectrometer Incoherent Scatter Radar Model: NRLMSIS 2.0

This study uses the publicly available mass spectrometer incoherent scatter radar model (NRLMSIS 2.0; Emmert et al., 2021) developed at the United States Naval Research Laboratory. The model uses an extensive database of observations from satellites, rockets, and radars since 1961. The model estimates atmospheric neutral temperature, composition, and neutral mass density from the ground to the exosphere. In this study, we use $F_{10.7}$ on the previous day and the 81-day centered mean $\overline{F}_{10.7}$, and daily Ap to specify the model inputs for solar and geomagnetic activity, respectively.

2.3 HASDM

The HASDM neutral mass density database is available for scientific use Tobiska et al. (2021). The HASDM neutral mass density is a correction to the JB2008 model Bowman et al. (2008) obtained by assimilating data from over 70 calibration satellites orbiting in the 190–900 km altitude range Tobiska et al. (2021). The tracking data for the calibration satellites are not publicly available. Of particular relevance to this study, CHAMP accelerometer-derived neutral mass density data from 2001 to 2005 is one of the data sources used to develop JB2008. JB2008 uses four different solar indices to represent the solar UV radiation absorbed in the thermosphere. These include the proxy index $F_{10.7}$, and indices based on measurements of 26–34 nm solar extreme ultraviolet emissions, magnesium-two h and k resonance lines, and 0.1–0.8 nm solar x-ray and Lyman-α emissions (see descriptions of $\mathrm{F_{10}}$, $\mathrm{S_{10}}$, $\mathrm{M_{10}}$, and $\mathrm{Y_{10}}$ in Bowman et al. (2008)). The model uses the 3-hr ap and Dst (disturbance storm time) indices to parameterize the energy deposited in the thermosphere due to geomagnetic activity. Tobiska et al. (2021) report that the uncertainty of HASDM is generally less than 5% compared to the neutral mass densities determined for the calibration satellites. The HASDM data set has a time resolution of 180 minutes, a horizontal resolution of 10°×15° in latitude and longitude, and a vertical resolution of 25 km.

3 Method

3.1 Estimating the Error Variance of Data

This work applies Grubbs (1948)' method of using four measurements of the same physical quantity to estimate the error variance of the measurement. This section briefly summarizes the method and its assumptions.

A measurement of a physical quantity consists of its true value T and the error of the measurement E. Consider four different instruments A, B, C, and D making the same measurement, whose recorded values consist of the truth T and some error E (e.g., $\mathrm{A} = \mathrm{T} + \mathrm{E_A}; \mathrm{B} = \mathrm{T} + \mathrm{E_B}$, and so forth). It follows from Grubbs (1948) that the error variance of, for example, $\mathrm{E_A}$ can be estimated independently of the true value T by working with the variance of the differences between pairs of instruments. For example, the variance of the difference between A and B is,

$$\mathrm{Var(A-B)} = \frac{1}{\mathrm{n}}\sum_{\mathrm{i}=1}^{\mathrm{n}}(\mathrm{A_i}-\mathrm{B_i})^2 - \big\langle \mathrm{A}-\mathrm{B}\big\rangle^2, \quad (2)$$

where the first (second) term on the right-hand side is the mean-square difference (mean bias) between the A and B measurements, and n is the sample size. And $\mathrm{Var(A-B)} \equiv \mathrm{Var(B-A)}$. Equation 22 in Grubbs (1948) describes this error variance relationship, simplified as follows:

$$\sigma(\mathrm{E_A}) = \sqrt{\mathrm{Var}(\mathrm{E_A})}$$
$$= \left\{ \frac{1}{3}\Big(\mathrm{Var(A-B)} + \mathrm{Var(A-C)} + \mathrm{Var(A-D)}\Big) \right.$$
$$\left. -\frac{1}{6}\Big(\mathrm{Var(B-C)} + \mathrm{Var(B-D)} + \mathrm{Var(C-D)}\Big) \right\}^{\frac{1}{2}}. \quad (3)$$

$\sigma(\mathrm{E_A})$ is the error standard deviation of $\mathrm{E_A}$. The variance terms $\mathrm{Var}(\cdot)$ on the right-hand side refers to the sample

variance (e.g., $\mathrm{Var(A-B)}$ is the variance of the difference between A and B measurements).

The Grubbs (1948)' method assumes that the true value T of the physical quantity is statistically independent of the error E of its measurement. The method also assumes that E from different instruments are also statistically independent of each other—zero error-covariance. In addition to these assumptions, sample size, significant outliers, and significant differences between the errors of different instruments may limit the accuracy of the method. Sjoberg et al. (2021) provide a discussion of these limitations and show results from an application of a variant of this method (using two and three data sets instead of four) to geophysical data.

3.2 Evaluation Metrics

We use the mean deviation $\Delta\rho$ to summarize the overall model performance. Here, $\Delta\rho$ is expressed as a percentage of the data-model difference relative to the observed value as follows:

$$\Delta\rho = \frac{1}{n}\sum_{i=1}^{n}\left(\left|\frac{\mathrm{Obs_i}-\mathrm{Mod_i}}{\mathrm{Obs_i}}\right|\cdot 100\right), \tag{4}$$

where n is the sample size, and Obs and Mod are the observation and model estimates, respectively. In a multimodel comparison, the model with the lowest $\Delta\rho$ has the best average agreement with the observations. The root-mean-square error (RMSE) is used to show how well the model captures the range of neutral mass density values in the data. The RMSE is $\sqrt{\frac{1}{n}\sum_{i=1}^{n}\left(\mathrm{Obs_i}-\mathrm{Mod_i}\right)^2}$.

In addition, we report the statistics of the mean ratio between the data sets d1 and d2 $\mu(\mathrm{d1/d2})$, and the standard deviation of the ratio $\sigma(\mathrm{d1/d2})$ defined as follows:

$$\mu(\mathrm{d1/d2}) = \exp\left(\frac{1}{\mathrm{n}}\sum_{\mathrm{i=1}}^{\mathrm{n}}\ln\frac{\mathrm{d1_i}}{\mathrm{d2_i}}\right), \tag{5}$$

$$\sigma(\mathrm{d1/d2}) = \sqrt{\frac{1}{\mathrm{n}}\sum_{\mathrm{i=1}}^{\mathrm{n}}\left(\ln\frac{\mathrm{d1_i}}{\mathrm{d2_i}}-\ln\mu(\mathrm{d1/d2})\right)^2}. \tag{6}$$

4 Results

4.1 CHAMP Accelerometer-Derived Neutral Mass Density

4.1.1 Differences in Neutral Mass Density Estimates Along CHAMP

In this section, we focus on the following accelerometer-derived neutral mass density products from CHAMP: Mehta et al. (2017) (PM), Sutton (2011) (ES), and Doornbos (2012) (TU). The differences between CHAMP-PM and -TU are due to the differences in accelerometer calibration parameters, aerodynamic modeling, and assumptions about neutral winds March et al. (2019); Mehta et al. (2017). While CHAMP-TU accounts for the contribution of winds to atmospheric drag, both CHAMP-PM and -ES neglect this contribution altogether. Mehta et al. (2017) attribute the bias between CHAMP-PM and -ES mainly to the use of a more correct model of the satellite geometry (exterior shape) in CHAMP-PM as well as the use of a fixed energy-accommodation-coefficient α_{E} in CHAMP-ES. Said differently, CHAMP-PM is a scaled version of CHAMP-ES. The α_{E} defines the energy loss due to the energy and momentum exchange between the satellite exterior and the surrounding air. Thus, α_{E} is a quantity that varies with, for example, solar activity, orbital altitude, and satellite surface material (March et al., 2019, and references therein). The α_{E} may significantly affect the drag coefficient $\mathrm{C_d}$, which is needed to calculate the atmospheric drag via Equation 1 Mehta et al. (2017). Table 1 in Mehta et al. (2017) indicates that the difference between CHAMP-PM and -ES due to solar activity is approximately 3%—for example, 15% in 2002 (solar maximum) and 18% in 2008 (solar minimum). The individual contributions from α_{E} and errors in the satellite geometry to this difference between CHAMP-PM and -ES neutral mass densities is not clear.

In CHAMP-PM, Mehta et al. (2017) apply a $\mathrm{C_d}$ that is about 10–12% smaller than the $\mathrm{C_d}$ in CHAMP-ES. Since neutral mass density is inversely proportional to $\mathrm{C_d}$ (see Equation 1), Mehta et al. (2017) attribute the primary reason for larger neutral mass densities in CHAMP-ES than CHAMP-PM to the increase in effective cross-sectional area. March et al. (2019) provide a detailed comparison of six different CHAMP geometry models and demonstrate that the along-track area projection of CHAMP is approximately 40% smaller in the geometry model used in CHAMP-ES than their high-fidelity geometry model. Liu et al. (2005) pointed out this problem of not accurately accounting for cross-sectional area several years before the release of the CHAMP-ES data, and revealed that using a simple panel geometry can produce neutral mass densities 30% larger than a more realistic shape.

Figures 1a and 2a show the accelerometer-derived neutral mass densities from CHAMP as estimated by Doornbos (2012) (TU; black), Mehta et al. (2017) (PM; gold), and Sutton (2011) (ES; orange) for the time periods 1 June–31 July 2003 and 2007, respectively. These arbitrary two-month periods provide a reasonably large sample for the ensuing statistical analysis in section 4.2. These data sets, limited as such, but with no significant data gaps, also help to avoid a skewed distribution (e.g., mixing of different seasonal and annual effects) that might affect the statistics. The two figures also show the neutral mass density estimates from TIE-GCM (gray), HASDM (blue), and NRLMSIS 2.0 (indigo) along the orbit corresponding to CHAMP-TU (section 4.1.2 describes some differences in the satellite location between the different CHAMP data products). Figures 1 and 2 also show the geophysical indices $F_{10.7}$, Dst, ap, and Kp to illustrate the space

weather conditions during the respective time periods (section 2 describes the use of these indices in the models).

Figures 1 and 2 indicate a persistent offset between CHAMP-ES and CHAMP-TU/PM in the orbit-averaged neutral mass densities during both high and low solar activity time periods. As summarized in Table 1, the mean ratio (Equation 5) between CHAMP-TU and -PM is 1.00 and 1.03 for 2003 and 2007, respectively. The mean ratio between CHAMP-TU and -ES is 0.84 (0.85) for 2003 (2007). The standard deviation of the ratio (Equation 6) between CHAMP-TU and -PM is 0.041 and 0.094 for 2003 and 2007, respectively. The standard deviation of the ratio between CHAMP-TU and -ES is 0.047 (0.093) for 2003 (2007). Thus, the systematic bias between CHAMP-ES and CHAMP-TU/PM show no significant dependence on solar activity. But their variance is higher during the solar minimum period of 2007 compared to 2003. In both figures, CHAMP-TU mostly overlaps with CHAMP-PM, except for some minor differences.

Figure 1 shows a few instances of neutral mass density enhancements in the CHAMP data, for example, 2, 10, and 18 June, and 12, 17, and 27 July 2003. Figure 1 displays that these six events correspond to the increased geomagnetic activity indicated by the Dst index in panel 1c. Figure 1 illustrates the nonlinear relationship between geomagnetic activity indices and orbit-averaged CHAMP data. For example, the nonproportionality of the amplitude differences of the peaks in the CHAMP data corresponding to the Dst index on 27 and 30 July 2003. The Kp (ap) index corresponding to these six events is above 5 (50 nT). Kp in panel 1f is above 5 at other times in addition to these six events. However, the proportional enhancement in neutral mass density for these other times is not as pronounced in the orbit-averaged CHAMP data (e.g., 29 and 31 July 2003). The comparison of $F_{10.7}$ and Dst on 10 and 18 June 2003 provides a good example of the significant neutral mass density enhancements caused by large energy deposition in a short period of time due to enhanced geomagnetic activity—the $F_{10.7}$ is above 180 sfu around 10 June 2003 and drops to approximately 120 sfu on 18 June 2003, while the change in Dst is about 3 times between the two days. Figure 2 also highlights the correspondence between the geomagnetic activity indices and neutral mass density peaks in the CHAMP data. The comparison also shows the influence of solar radiation—the general decreasing trend in neutral mass density from 10 to 21 June 2007 corresponds to the decrease in $F_{10.7}$.

Moreover, Figure 1 shows the potential impact of these indices on model estimates. For example, HASDM, which uses both ap and Dst indices captures the trend in neutral mass density enhancement on 2 June 2003 better than both NRLMSIS 2.0 and TIE-GCM, which use ap and Kp, respectively. As another example, HASDM reproduces the multiple peaks seen in the CHAMP data during 28–29 June 2003, while TIE-GCM shows only a single peak and NRLMSIS 2.0 shows none. Similar trend differences between model estimates are seen during 25–27 July 2003. The sudden drop in neutral mass density on 23 June 2003 visible in the CHAMP data as well as in all model estimates, is due to averaging over a brief time period of missing data. As with Figure 1, Figure 2 demonstrates some important trend differences among the model estimates. These trend differences highlight the challenges of modeling neutral mass density dynamics.

Figure 3 summarizes the performance of the three models used in this study relative to the CHAMP data. Figures 3a and 3b quantify this performance as the mean percentage-deviation $\Delta\rho$ considering both CHAMP-TU (dotted-bar) and -ES (plain bar) separately as Obs in Equation 4. The $\Delta\rho$ statistics for CHAMP-PM (not shown) are similar to those for CHAMP-TU. In addition, Figures 3c and 3d provide the RMSE results of the models.

Figures 3a and 3b show that the mean percentage-deviation of TIE-GCM does not vary much between CHAMP-TU and -ES. Both NRLMSIS 2.0 and HASDM have a markedly larger $\Delta\rho$ with CHAMP-TU than with CHAMP-ES. All models have a better average agreement with CHAMP data during the high solar activity period in 2003 than during the low solar activity period in 2007. Relative to CHAMP-TU, TIE-GCM has the lowest RMSE during both time periods (Figures 3c and 3d). HASDM, on the other hand, has the best RMSE statistics relative to CHAMP-ES. In general, the RMSE value is smaller in 2007 compared to 2003 for all the models except for NRLMSIS 2.0 relative to CHAMP-TU.

The data-model comparison in Figures 1–3 shows that the models capture the variability seen in the data quite well. The ratio statistics in Table 1 show that, on average, all three models tend to overestimate ($\mu < 1$) in both 2003 and 2007. This overestimation is slightly higher in 2007 and more pronounced in HASDM and NRLMSIS 2.0 than in TIE-GCM. The σ values of the three models in Table 1 do not change much between 2003 and 2007—indicating that the data-model variance is persistent and less dependent on solar activity. Thus, given the differences between CHAMP-TU and -ES, it is reasonable to use these model estimates to calculate the error standard deviation as described in section 3.1.

4.1.2 Differences in Orbital Heights Estimated for CHAMP

In this section, we point out that in addition to the differences in neutral mass density between the three CHAMP data sets, there are also some discrepancies in the satellite heights in the published data. We demonstrate this in Figures 4 and 5 by comparing the standard deviation of the orbital heights reported in four different CHAMP products: Rother and Michaelis, 2019 (GFZ), Doornbos, 2012 (TU), Mehta et al., 2017 (PM), and Sutton, 2011 (ES) for the time period 1 June–31 July 2003. The two figures show the standard deviation as a function of 3° in geographic latitude and 1 hour in local time.

The notable feature in Figures 4 and 5 is the dissimilarity of CHAMP-ES compared to the other three CHAMP products. The differences in CHAMP-ES may be a result of the latitude binning used in the processing of the data by Sutton (2011). The data release-note for CHAMP-ES

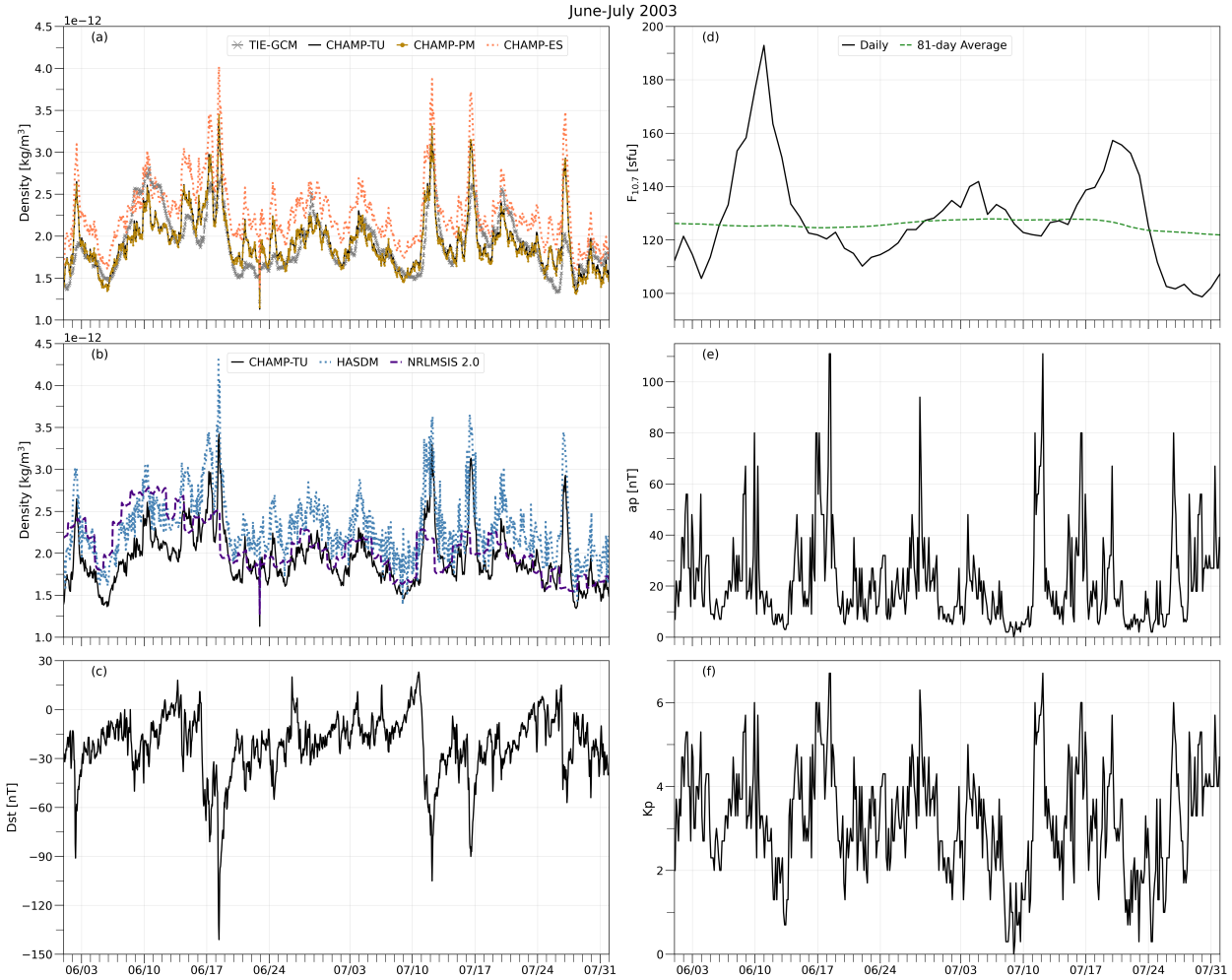

Figure 1: (a–b) Orbit-averaged accelerometer-derived neutral mass densities from the CHAllenging Minisatellite Payload (CHAMP) mission as estimated by Doornbos (2012) (TU), Mehta et al. (2017) (PM), and Sutton (2011) (ES) during 1 June–31 July 2003. Estimates from the HASDM Tobiska et al. (2021), NRLMSIS 2.0 Emmert et al. (2021), and physics-based TIE-GCM are along the orbit corresponding to CHAMP-TU. (c-f) Space weather conditions demonstrated via Dst, $F_{10.7}$, 3-hour ap and Kp. $1\,\text{sfu} = 10^{-22} \cdot \text{W} \cdot \text{m}^{-2} \cdot \text{Hz}^{-1}$.

Table 1: *The ratio statistics of the data sets with CHAMP-TU as d1 in Equations 5 and 6. The sample sizes correspond to the respective distributions in Figures 1 and 2.*

	2003		2007	
d2	$\mu(\text{d1}/\text{d2})$	$\sigma(\text{d1}/\text{d2})$	$\mu(\text{d1}/\text{d2})$	$\sigma(\text{d1}/\text{d2})$
CHAMP-PM	1.00	0.041	1.03	0.094
CHAMP-ES	0.84	0.047	0.85	0.093
TIE-GCM	0.96	0.223	0.90	0.237
HASDM	0.83	0.215	0.77	0.241
NRLMSIS 2.0	0.91	0.222	0.76	0.259

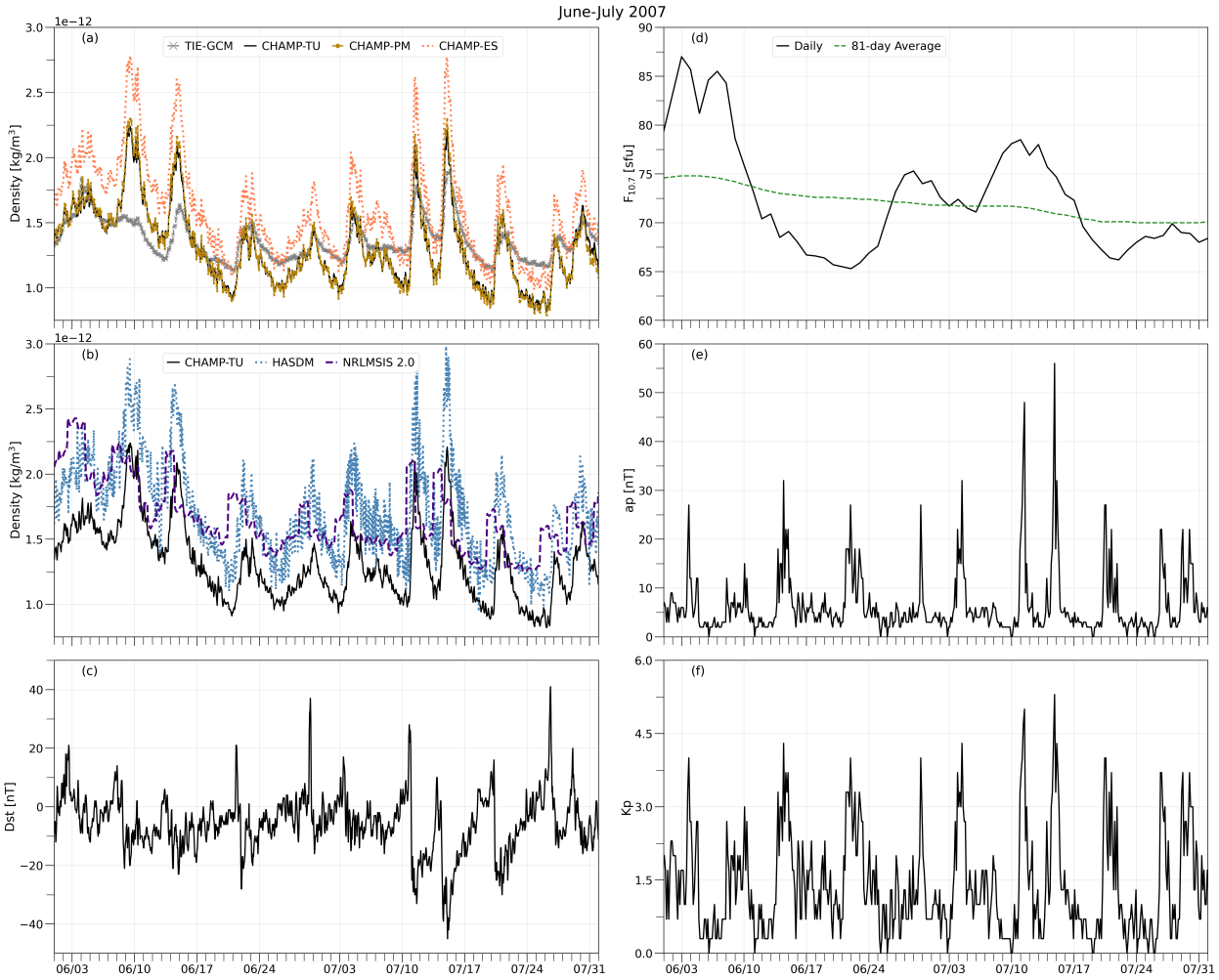

Figure 2: (a–f) Same as Figure 1 except for 2007.

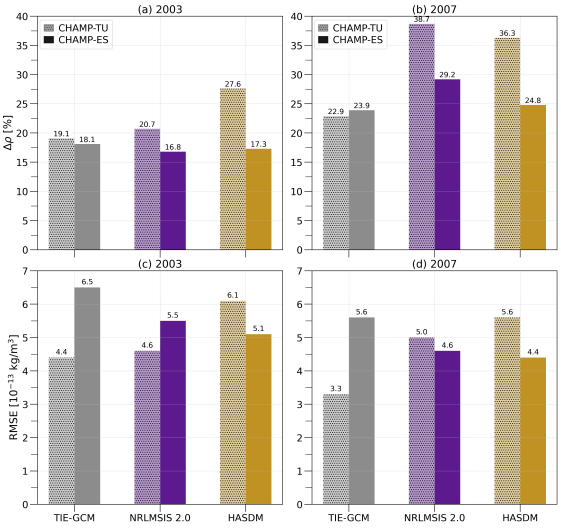

Figure 3: (a, b) The mean percentage-deviation ($\Delta\rho$) of neutral mass density relative to Doornbos (2012) CHAMP-TU (dotted-bar) and Sutton (2011) CHAMP-ES (plain bar) calculated as per Equation 4. The values printed on each bar indicate the exact $\Delta\rho$. (c, d) The root-mean-square error (RMSE) of the models. The results correspond to the time periods 1 June–31 July 2003 (a and c), and 2007 (b and d).

version 2.3 states that this bin width is 3° in latitude and that they discard the bins with no data. The standard deviations for CHAMP-TU, -PM, and -GFZ in the two figures are strikingly similar except for some minor differences.

4.2 Estimating the Error in CHAMP Neutral Mass Density

Figure 6 presents the latitudinal variation of the estimated error standard deviation $\sigma(\mathrm{E_A})$ (see section 3.1) of the CHAMP data sets and models. Figure 6a (b) concerns the time period in Figure 1 (2). The sample size of each data set in both time periods is approximately 176000 epochs. For reference, Figure 6 also shows the errors estimated by Sutton (2011) for the CHAMP-ES data set (orange-dotted line shown as *Sutton 2011*; see section 3 in Sutton et al. (2007) for details). Table 2 describes the data set combinations used with a given data set as A in Equation 3. Table 3 summarizes these estimated error standard deviations.

First we focus on the estimated error standard deviations of CHAMP-TU, -PM, and -ES. Figure 6a shows that the difference between $\sigma(\mathrm{E_A})$ for CHAMP-TU and -ES increases up to about 4% in the low-middle latitudes. In the high latitudes above 60° N/S, their error percentages are relatively higher but similar to each other. In contrast to 2003, Figure 6b shows a considerable offset between the error distributions of CHAMP-TU and -PM in 2007. While $\sigma(\mathrm{E_A})$ for CHAMP-PM closely follows CHAMP-TU in 2003, the errors of CHAMP-PM are relatively larger in 2007 and closer to those of CHAMP-ES, especially in the Southern Hemisphere. The median error in 2003 is 2.1, 5,

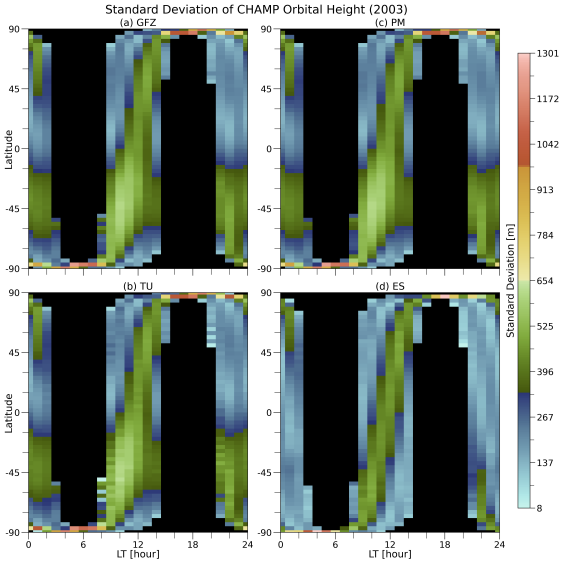

Figure 4: The standard deviation of the height of the CHAllenging Minisatellite Payload (CHAMP) satellite as a function of geographic latitude and local time. The data correspond to the time period 1 June–31 July 2003 as reported in (a) Rother and Michaelis, 2019 (GFZ), (b) Doornbos, 2012 (TU), (c) Mehta et al., 2017 (PM), and (d) Sutton, 2011 (ES). The bin size is 3° in geographic latitude and 1-hr in local time.

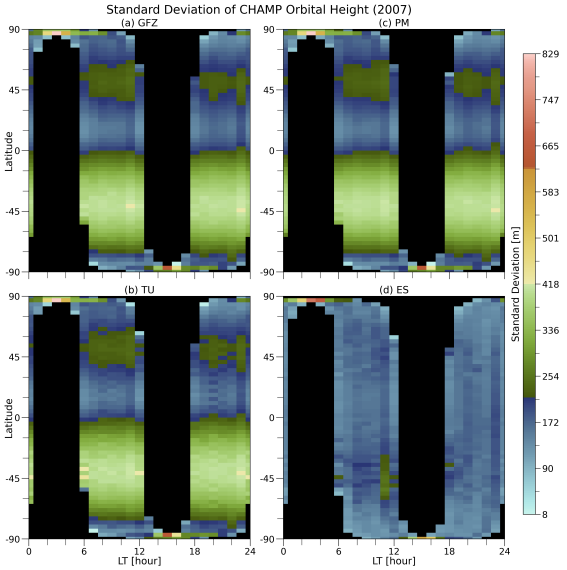

Figure 5: Same as Figure 4 except for 2007.

Table 2: *The data sets used in place of A, B, C, and D in Equation 3 for the $\sigma(\mathrm{E_A})$ values present in Figure 6.*

A	B	C	D
CHAMP-TU	TIE-GCM	HASDM	NRLMSIS 2.0
CHAMP-PM	TIE-GCM	HASDM	NRLMSIS 2.0
CHAMP-ES	TIE-GCM	HASDM	NRLMSIS 2.0
HASDM	CHAMP-TU(-ES)	TIE-GCM	NRLMSIS 2.0
NRLMSIS 2.0	CHAMP-TU(-ES)	HASDM	TIE-GCM
TIE-GCM	CHAMP-TU(-ES)	HASDM	NRLMSIS 2.0

Note: Figure 6 shows $\sigma(\mathrm{E_A})$ results for the three models with B replaced by CHAMP-TU and -ES separately.

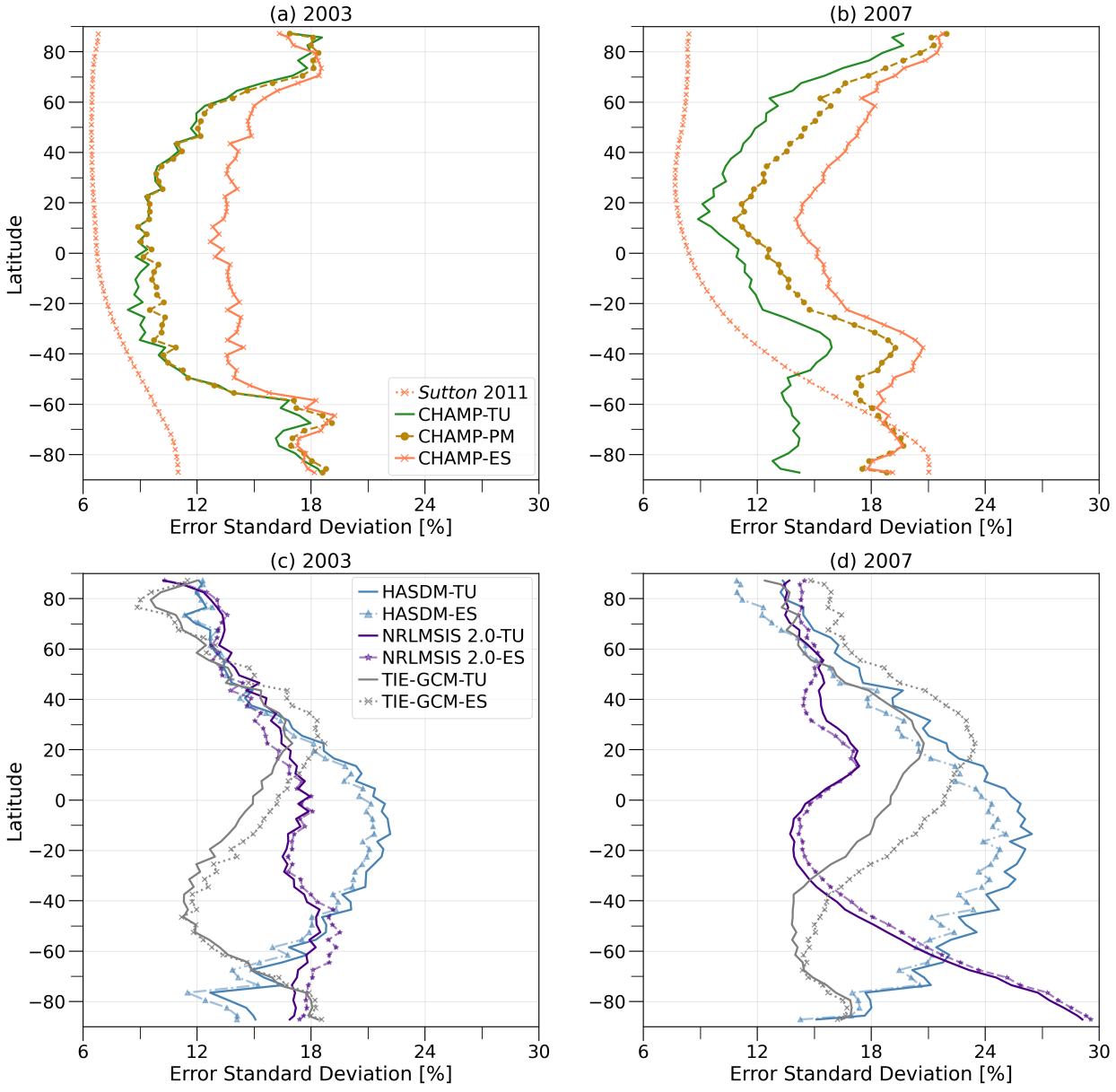

Figure 6: Estimated error standard deviation $\sigma(\mathrm{E_A})$ [%] as a function of geographic latitude (positive Northern Hemisphere) for the neutral mass density data sets considered in this study during (a, c) 2003 and (b, d) 2007. Here, we treat each specified data set separately as A in Equation 3. In panels (c) and (d), each model name followed by TU (ES) indicates that the B data set used in Equation 3 is CHAMP-TU (-ES) (see Table 2). In panels (a) and (b), *Sutton 2011* (orange-dotted) refers to the errors estimated by Sutton (2011) for the CHAMP-ES data set.

Table 3: *Summary statistics for the estimated error standard deviation* $\sigma(\mathrm{E_A})$ *in Figure 6. All* $\sigma(\mathrm{E_A})$ *values are in units of* $10^{-13}\mathrm{kg/m^3}$. *The values in bold give* $\sigma(\mathrm{E_A})$ *as a percentage.*

$\sigma(\mathrm{E_A})$	minimum (%)	maximum (%)	median (%)
2003			
CHAMP-TU	1.46 (**8.4**)	4.36 (**18.6**)	2.07 (**11.0**)
CHAMP-PM	1.50 (**8.9**)	4.22 (**19.1**)	2.13 (**11.2**)
CHAMP-ES	2.13 (**12.7**)	5.13 (**19.2**)	3.56 (**14.3**)
HASDM-TU	1.53 (**11.4**)	5.94 (**22.2**)	3.83 (**16.9**)
HASDM-ES	1.38 (**11.3**)	5.76 (**21.3**)	3.83 (**16.5**)
NRLMSIS 2.0-TU	2.05 (**10.2**)	4.45 (**18.5**)	3.22 (**16.9**)
NRLMSIS 2.0-ES	2.12 (**10.3**)	4.41 (**19.5**)	3.17 (**17.0**)
TIE-GCM-TU	1.77 (**9.6**)	3.90 (**18.4**)	2.45 (**13.6**)
TIE-GCM-ES	1.76 (**8.8**)	4.29 (**18.7**)	2.57 (**14.7**)
*Sutton 2011**	1.29 (**6.4**)	1.84 (**11.0**)	1.77 (**6.8**)
2007			
CHAMP-TU	0.77 (**8.9**)	3.29 (**19.7**)	1.63 (**13.1**)
CHAMP-PM	0.90 (**10.8**)	3.86 (**21.9**)	1.90 (**16.2**)
CHAMP-ES	1.11 (**14.0**)	4.64 (**21.7**)	2.82 (**18.0**)
HASDM-TU	1.30 (**13.2**)	5.30 (**26.5**)	3.52 (**21.3**)
HASDM-ES	1.23 (**10.9**)	4.99 (**25.1**)	3.27 (**20.4**)
NRLMSIS 2.0-TU	2.02 (**13.4**)	3.58 (**29.1**)	2.67 (**15.5**)
NRLMSIS 2.0-ES	2.11 (**14.2**)	3.54 (**29.6**)	2.81 (**15.4**)
TIE-GCM-TU	1.19 (**12.4**)	3.67 (**20.8**)	2.17 (**16.0**)
TIE-GCM-ES	1.18 (**14.4**)	4.14 (**23.4**)	2.52 (**16.9**)
*Sutton 2011**	1.29 (**7.7**)	1.77 (**21.0**)	1.56 (**8.4**)

Note: *Sutton 2011* refers to the errors estimated by Sutton (2011) for the CHAMP-ES data set. Each model name followed by TU or ES indicate the B data set used in Equation 3 (see Table 2).

and 3.7% smaller for CHAMP-TU, -PM, and -ES, respectively, compared to 2007. The higher signal-to-noise ratio of accelerometer measurements in LEO during periods of high solar activity may contribute to the low errors found here. This demonstrates that the rescaling approach used in CHAMP-PM by Mehta et al. (2017) is more effective in reducing the uncertainty during the high solar activity period of 2003 than in 2007.

Figure 6 shows that among the data sets used in this study (Table 2), CHAMP-TU has the lowest median error during the two time periods. Table 3 indicates that the minimum-maximum error range for each CHAMP data set does not vary much between the two time periods in 2003 and 2007 (approximately 0.6–1.2%). The latitudinal trends between the three CHAMP data sets are mostly similar in each time period. In general, the error estimates for the CHAMP data are smaller at low latitudes compared to high latitudes. In the southern latitudes, the $\sigma(\mathrm{E_A})$ values for the three CHAMP data sets peak around 60-70° S (40° S) in 2003 (2007).

The *Sutton 2011* errors estimated by Sutton (2011) for the CHAMP-ES data set do not show much difference in the trends between the two time periods in Figure 6—low errors in northern latitudes and errors that gradually increase toward southern high latitudes. The latitudinal trend in *Sutton 2011* errors is markedly different from that of $\sigma(\mathrm{E_A})$ for CHAMP-ES. Except in the southern high latitudes in 2007, the magnitude of *Sutton 2011* errors is significantly smaller than that of $\sigma(\mathrm{E_A})$ for CHAMP-ES. The *Sutton 2011* errors indicate that the uncertainty in the northern polar latitudes is as small as in the northern low and middle latitudes.

Figures 6c and 6d focus on the estimated error standard deviations of the three models. Here, we present the $\sigma(\mathrm{E_A})$ results of the models in two configurations: with CHAMP-TU and -ES separately as the B data set in Equation 3. This provides a test of the reliability of the error estimates and shows the effect of using different combinations of data sets on $\sigma(\mathrm{E_A})$. It is evident from Figures 6c and 6d that the effect of using CHAMP-TU or -ES on the latitudinal trends of the model errors is negligible. The two figures highlight that it does, however, affect the magnitude of the estimated errors of the TIE-GCM at low latitudes more than those of other models. Table 3 shows that in 2003 (2007) the change in the minimum-maximum error range between the TU-ES configurations for TIE-GCM, NRLMSIS 2.0, and HASDM is 1.1, 0.9, and 0.8% (0.6, 0.3, 0.9%), respectively. In 2003 (2007), the change in median error between the TU-ES configurations for TIE-GCM, NRLMSIS 2.0, and HASDM is 1.1, 0.1, and 0.4% (0.9, 0.1, 0.9%), respectively.

In Table 3, among the models used in this study, TIE-GCM (NRLMSIS 2.0) has the lowest median $\sigma(\mathrm{E_A})$ for 2003 (2007). And Figure 6c shows that all three models have similar error distributions in both trend and magnitude in the Northern Hemisphere above 20° N. In Figures 6a and 6c, while the error estimates for the models are lower than those from the CHAMP data in the northern high latitudes above 60° N, they are mostly similar in the southern high latitudes above 60° S.

The results indicate that HASDM has a larger error spread (minimum-maximum range above 10%) than other models in both time periods. Figure 6 shows that the latitudinal trends in $\sigma(\mathrm{E_A})$ for HASDM are similar in 2003 and 2007, and their magnitude increases almost linearly from the poles to the equator. The large errors in HASDM may be due to the processing of the HASDM data, which have considerably large spatial and temporal resolutions (see section 2.3). In 2007, in the latitude range approximately between 60° S and 60° N, $\sigma(\mathrm{E_A})$ for NRLMSIS 2.0 is close to the error estimates for CHAMP data—and mostly less than $\sigma(\mathrm{E_A})$ for CHAMP-ES. Interestingly, the NRLMSIS 2.0 error has a high gradient south of 20° S (Figure 6d).

5 Discussion

We begin with a detailed look at three of the widely used CHAMP accelerometer-derived neutral mass density products: Sutton (2011), Doornbos (2012), and Mehta et al. (2017), during a two-month period of high (2003) and low (2007) solar activity. In Figures 1 and 2, we highlight the differences between these CHAMP neutral mass density products derived from the same STAR accelerometer measurements using different methods. Mehta et al. (2017) show that CHAMP-PM is on average about 18% (5%) smaller (larger) than CHAMP-ES (-TU) in 2007. And in 2003, CHAMP-PM is about 16% (6%) smaller (larger) than CHAMP-ES (-TU). March et al. (2019) compare a few hours of these three neutral mass density products at different solar activity levels and report that CHAMP-ES generally has larger neutral mass densities compared to both CHAMP-TU and -PM. The comparisons in Figures 1 and 2 and Table 1 confirm that this offset between CHAMP-ES and CHAMP-TU/PM is persists during both high and low solar activity time periods.

The time series of CHAMP-PM in Figures 1 and 2 is mostly similar in trend and magnitude to that of CHAMP-TU. Figure 6 shows that $\sigma(\mathrm{E_A})$ for CHAMP-PM is also more similar to CHAMP-TU in 2003 and has some considerable differences in 2007. These differences between CHAMP-PM and -TU in 2007 may be due to certain assumptions in the data processing, such as the neglect of neutral winds in CHAMP-PM, which manifest more strongly in the data quality during periods of low solar activity when the signal-to-noise ratio in the accelerometer measurements is low March et al. (2019); Mehta et al. (2017). Although Doornbos (2012) uses neutral winds from Drob et al. (2008) horizontal wind model (HWM07) to derive CHAMP-TU, they also use accelerometer-derived neutral winds where possible March et al. (2019). The fraction of CHAMP-TU data derived with or without HWM07 is unclear. Some data assimilation experiments with, for example, HWM07 and Förster and Doornbos (2019) CHAMP cross-track winds may be useful to investigate the impact of these neutral winds on the quality of the neutral mass density estimates.

We use Equation 3 to compute the estimated error standard deviation $\sigma(\mathrm{E_A})$ of the CHAMP data according to the data set combination in Table 2. As shown in Equation 3, no instrument is specifically weighted and the order of the

B, C, and D instruments is irrelevant to the final result. As such, Equation 3 treats both data and model estimates equally, assuming that they represent the true neutral mass density with some unknown error. The latitudinal trends between the three CHAMP data sets in Figure 6 show that the error estimates are generally smaller at low latitudes compared to other regions. The percentage of error spread for the CHAMP data (minimum-maximum difference) is slightly larger during the low solar activity period in 2007 compared to 2003. This difference in error spread between 2003 and 2007 is twice as large for CHAMP-ES compared to CHAMP-TU (1.2 vs. 0.6%). The minimum-maximum error range estimated by Sutton (2011) for CHAMP-ES is 4.6% (13.3%) for 2003 (2007). An exact reason for this large difference in the minimum-maximum error range (8.7%), especially in the southern middle-high latitudes (Figure 6b), is difficult to identify.

Using early accelerometer measurements under quiet geomagnetic conditions (ap less than 15), Bruinsma et al. (2004) estimate an error of about 10–15% for CHAMP neutral mass density. Sutton et al. (2007), using data for one orbit, demonstrate that systematic errors are the largest contributor to the total error in CHAMP neutral mass density and estimate an error in the range of 6–15.6%. In Figure 6, we show that the errors estimated by Sutton (2011) for CHAMP-ES are somewhat smaller than our $\sigma(\mathrm{E_A})$ estimates. For example, as summarized in Table 3, our $\sigma(\mathrm{E_A})$ estimates for CHAMP-ES are in the range of 12.7–19.2% and *Sutton 2011* errors for the same period are in the range of 6.4–11.0%. Stolle and Liu (2014) describe that the estimated precision of CHAMP neutral mass density is approximately $1 \cdot 10^{-14}\mathrm{kg/cm^3}$. In Table 3, only CHAMP-TU and -PM have a minimum $\sigma(\mathrm{E_A})$ below $1 \cdot 10^{-13}\mathrm{kg/cm^3}$. While Sutton et al. (2007) provide a detailed error analysis, Bruinsma et al. (2004) and Stolle and Liu (2014) do not reveal the exact method used to compute these error estimates. In general, the error standard deviations for the CHAMP data sets estimated in this study are close to the uncertainties reported in Bruinsma et al. (2004) and Sutton et al. (2007). Consequently, our results demonstrate that the Grubbs (1948)' method (see section 3.1) provides realistic estimates of the uncertainty of CHAMP neutral mass density.

The assumptions about error correlations are important for the Grubbs (1948)' method. The variance of a quantity can be greater than or equal to zero but never negative. The Equation 3 makes it possible to have negative estimates for the error variance because it ignores the unknown error correlations between the different data sets. Thus, a negative error variance is possible if the sum of these error-covariance terms (e.g., $\mathrm{Cov(E_A,E_B)}$, $\mathrm{Cov(E_A,E_C)}$, etc.) is greater than the error variance itself Sjoberg et al. (2021). In reality, error correlations may exist between these different data sets—especially the three CHAMP data sets, which share the same raw accelerometer measurements. To minimize the effect of error correlations, we avoid using the three CHAMP data sets together in Equation 3. The HASDM is based on the JB2008 model, which was developed using CHAMP data, among others. Thus, the HASDM is a potential source of error correlations that could affect the accuracy of the error estimates presented here.

Since both the physics-based and the empirical models rely on similar driver parameters, such as $F_{10.7}$, Kp, and ap, it remains to be determined the possible error correlations between the models. Furthermore, spurious error correlations may occur, for example, when the sample size is small. While Sjoberg et al. (2021) recommend a sample size of 5000 (in a study using synthetic terrestrial weather data), further experimentation will be necessary to determine the critical sample size that yields meaningful estimates of error variance for accelerometer-derived neutral mass density data sets. It may be useful to explore methods to mitigate the impact of these error correlations on the estimated uncertainty, such as the statistical minimization techniques proposed by, for example, Tavella and Premoli (1994) and Galindo et al. (2001).

Figure 6 also presents an application of the Grubbs (1948)' method to estimate the error standard deviation of the models. The error estimates using both CHAMP-TU and -ES demonstrate the reliability of the method. The results show that the magnitude of $\sigma(\mathrm{E_A})$ does indeed change slightly (0.1–1.1%) when CHAMP-TU is replaced with CHAMP-ES. This exercise demonstrates that the effect of using CHAMP-TU or -ES on the latitudinal trends of the model errors is negligible. A notable feature in Figure 6d is the sharp increase in NRLMSIS 2.0 errors in the Southern Hemisphere. It remains to investigate the quality of the database used in NRLMSIS 2.0 to represent this southern latitude region in 2007. Emmert et al. (2021) describe the years 2005–2009 as anomalous solar minimum years and have removed these years from their comparisons with accelerometer-derived neutral mass densities. Figure 6 shows that the latitudinal trends in $\sigma(\mathrm{E_A})$ for HASDM are significantly different from those of the other two models. Although HASDM performs well against CHAMP-TU and -ES in Figure 3, it has a consistently large $\sigma(\mathrm{E_A})$ in the low-middle latitudes in Figure 6. We attribute this anomaly to data processing (see section 2.3). The relatively large temporal and spatial resolutions of the HASDM database may have contributed to its error characteristics in Figure 6. Lechtenberg et al. (2013), using CHAMP data among others, concluded that the resolution of HASDM is inadequate to sufficiently characterize short-term density perturbations, such as traveling atmospheric disturbances, geomagnetic cusp phenomena, and midnight density maxima.

6 Summary and Conclusions

This work examined three publicly available CHAMP accelerometer-derived neutral mass density products—Mehta et al. (2017) (PM), Sutton (2011) (ES), and Doornbos (2012) (TU), with the goal of describing their differences and identifying systematic errors. The work compared the CHAMP neutral mass density data sets with some common physical (TIE-GCM) and empirical (HASDM and NRLMSIS 2.0) models. And the compar-

isons covered the months of June and July in 2003 and 2007, corresponding to high and low solar activity time periods, respectively.

This paper is the first to apply the Grubbs (1948)' method to the error characterization of thermosphere data sets. The main results of this work concerning the error characteristics of neutral mass density are as follows:

1. The Grubbs (1948)' method provides reliable estimates of the uncertainty of the CHAMP neutral mass density;
2. The median error standard deviation $\sigma(\mathrm{E_A})$ for CHAMP-TU, -PM, and -ES vary approximately in the range 11.0–13.1, 11.2–16.2, and 14.3–18.0%, respectively;
3. CHAMP-TU has the lowest $\sigma(\mathrm{E_A})$ in the two study periods in 2003 and 2007;
4. The $\sigma(\mathrm{E_A})$ of the three models are generally larger than that of CHAMP-TU;
5. Among the models, TIE-GCM (NRLMSIS 2.0) has the lowest median $\sigma(\mathrm{E_A})$ for 2003 (2007);
6. A latitude dependence of $\sigma(\mathrm{E_A})$ is evident for both CHAMP data and models;
7. The $\sigma(\mathrm{E_A})$ for the CHAMP data are generally small at low-middle latitudes compared to high latitudes;
8. The $\sigma(\mathrm{E_A})$ for HASDM is considerably larger than TIE-GCM or NRLMSIS 2.0 at low-middle latitudes.

This work used several statistics to quantity the model performance. The data-to-model ratio indicated that on average, all three models tend to overestimate relative to CHAMP-TU—the overestimation is slightly higher during the low solar activity period in 2007 than in 2003. The findings showed that the variance of the data-model ratio was persistent and less sensitive to solar activity. In general, the models capture the variability seen in the data quite well. The mean percentage-deviation $\Delta\rho$ of the models is larger in 2007 than in 2003. In other words, the data-model agreement is better in 2003 than in 2007. The $\Delta\rho$ with CHAMP-TU is markedly larger than that with CHAMP-ES for both NRLMSIS 2.0 and HASDM. TIE-GCM (HASDM) has the best RMSE statistics compared to CHAMP-TU (-ES).

The differences between the three CHAMP data sets are systematic and persistent over the two time periods of this study. These differences are mainly due to the assumptions made in the different derivation methods. Thus, it is obvious that these assumptions have a significant impact on the error estimates. Among these publicly available CHAMP data sets, only CHAMP-ES provides error estimates. The $\sigma(\mathrm{E_A})$ is a useful quantity for understanding of the error distribution in the data. While CHAMP-TU has the lowest $\sigma(\mathrm{E_A})$ in our results, the user can experiment with other models and data sets to compute $\sigma(\mathrm{E_A})$ to gain a further understanding of the task specific errors. Ongoing recalibration efforts, such as, ESA's TOLEOS (thermosphere observations from low-Earth orbiting satellites) project, may consider incorporating error estimates for the various neutral mass density products, including CHAMP. This will be invaluable for the thermosphere model development and calibration work, as well as for data assimilation studies.

The promising results of this preliminary application of the Grubbs (1948)' method invite further work to investigate the applicability of the method to other data sets in the space weather and aeronomy community. For example, large data sets spanning over multiple years could be used to study the characteristics of error correlations between different measurements and under different geophysical conditions. The CHAMP, GRACE (gravity recovery and climate experiment; 2 satellites), GRACE-Follow-On (2 satellites), and Swarm (3 satellites) missions provide independent accelerometer-derived neutral mass densities. Thus, in the possible absence of error correlations between instruments, the Grubbs (1948)' method could be used to compare the error estimates in neutral mass density products from these satellites.

Open Research

All data and models used in this work are in the public domain, and can be reproduced as exactly as described in the paper. The Delft University of Technology (<ftp://thermosphere.tudelft.nl>) provided the CHAMP-TU data (version v01). Mehta et al. (2017) provided the CHAMP-PM and -ES data via <http://tinyurl.com/densitysets>. The UCAR/HAO (<www.hao.ucar.edu/modeling/tgcm>) provided the TIE-GCM code. Space Environment Technologies (<spacewx.com/hasdm>) provided the HASDM neutral mass density data. The United States Naval Research Laboratory (<map.nrl.navy.mil/map/pub/nrl/NRLMSIS>) provided the NRLMSIS 2.0. The NASA/OMNI database (<omniweb.gsfc.nasa.gov>) provided the Kp, ap, Dst, and $F_{10.7}$ measurements.

Acknowledgments

The German Aerospace Center (<www.dlr.de>) funded the CHAMP mission through the Federal Ministry of Economics and Technology, following a decision of the German Federal Parliament (grant code 50EE0944).

References

European Space Agency. *ESA's Annual Space Environment Report*. ESA Space Debris Office, Darmstadt, 2021. Ref: GEN-DB-LOG-00288-OPS-SD.

J.T. Emmert, H.P. Warren, A.M. Segerman, J.M. Byers, and J.M. Picone. Propagation of atmospheric density errors to satellite orbits. *Advances in Space Research*, 59(1):147–165, 2017. ISSN 0273-1177. doi: 10.1016/j.asr.2016.07.036.

M. D. Hejduk and D. E. Snow. The effect of neutral density estimation errors on satellite conjunction serious

event rates. *Space Weather*, 16(7):849–869, 2018. doi: 10.1029/2017SW001720.

David A. Vallado and David Finkleman. A critical assessment of satellite drag and atmospheric density modeling. *Acta Astronautica*, 95:141–165, 2014. doi: 10.1016/j.actaastro.2013.10.005.

Timothy Kodikara, Brett Carter, and Kefei Zhang. The first comparison between Swarm-C accelerometer-derived thermospheric densities and physical and empirical model estimates. *Journal of Geophysical Research: Space Physics*, 123(6):5068–5086, 2018. doi: 10.1029/2017JA025118.

P. M. Mehta, A. C. Walker, E. K. Sutton, and H. C. Godinez. New density estimates derived using accelerometers on board the CHAMP and GRACE satellites. *Space Weather*, 15(4):558–576, 2017. doi: 10.1002/2016SW001562.

Alexey V. Morozov, Aaron J. Ridley, Dennis S. Bernstein, Nancy Collins, Timothy J. Hoar, and Jeffrey L. Anderson. Data assimilation and driver estimation for the global ionosphere-thermosphere model using the ensemble adjustment kalman filter. *Journal of Atmospheric and Solar-Terrestrial Physics*, 104:126–136, 2013. ISSN 1364-6826. doi: 10.1016/j.jastp.2013.08.016.

J. S. Shim, M. Kuznetsova, L. Rastätter, D. Bilitza, M. Butala, M. Codrescu, B. A. Emery, B. Foster, T. J. Fuller-Rowell, J. Huba, A. J. Mannucci, X. Pi, A. Ridley, L. Scherliess, R. W. Schunk, J. J. Sojka, P. Stephens, D. C. Thompson, D. Weimer, L. Zhu, and E. Sutton. CEDAR Electrodynamics Thermosphere Ionosphere (ETI) Challenge for systematic assessment of ionosphere/thermosphere models: Electron density, neutral density, NmF2, and hmF2 using space based observations. *Space Weather*, 10(10), 2012. doi: 10.1029/2012SW000851.

Eric K. Sutton. A new method of physics-based data assimilation for the quiet and disturbed thermosphere. *Space Weather*, 16(6):736–753, 2018. doi: 10.1002/2017SW001785.

Charles D. Bussy-Virat, Aaron J. Ridley, and Joel W. Getchius. Effects of uncertainties in the atmospheric density on the probability of collision between space objects. *Space Weather*, 16(5):519–537, 2018. doi: 10.1029/2017SW001705.

B. R. Bowman, K.W. Tobiska, F. A. Marcos, C. Y. Huang, C. Lin, and W. F. Burke. A new empirical thermospheric density model JB2008 using new solar and geomagnetic indices. *Proceedings of the AIAA/AAS Astrodynamics Specialist Conference, 18-21 August 2008, Honolulu, Hawaii*, 2008–6438, 2008. doi: 10.2514/6.2008-6438.

D. R. Weimer, E. K. Sutton, M. G. Mlynczak, and L. A. Hunt. Intercalibration of neutral density measurements for mapping the thermosphere. *Journal of Geophysical Research: Space Physics*, 121(6):5975–5990, 2016. doi: 10.1002/2016JA022691.

G. March, E.N. Doornbos, and P.N.A.M. Visser. High-fidelity geometry models for improving the consistency of CHAMP, GRACE, GOCE and swarm thermospheric density data sets. *Advances in Space Research*, 63(1):213–238, 2019. ISSN 0273-1177. doi: 10.1016/j.asr.2018.07.009.

W. Kent Tobiska, Bruce R. Bowman, S. David Bouwer, Alfredo Cruz, Kaiya Wahl, Marcin D. Pilinski, Piyush M. Mehta, and Richard J. Licata. The set hasdm density database. *Space Weather*, 19(4):e2020SW002682, 2021. doi: 10.1029/2020SW002682.

David R. Jackson, Sean Bruinsma, Sandra Negrin, Claudia Stolle, Chris J. Budd, Raul Dominguez Gonzalez, Emily Down, Daniel J. Griffin, Matthew J. Griffith, Guram Kervalishvili, Daniel Lubián Arenillas, James Manners, Jürgen Matzka, Yuri Y. Shprits, Ruggero Vasile, and Irina S. Zhelavskaya. The space weather atmosphere models and indices (SWAMI) project: Overview and first results. *J. Space Weather Space Clim.*, 10:18, 2020. doi: 10.1051/swsc/2020019.

Claudia Stolle and Huixin Liu. Low-latitude ionosphere and thermosphere: Decadal observations from the CHAMP mission. In *Modeling the Ionosphere Thermosphere System*, chapter 21, pages 259–272. John Wiley, Washington, 2014. ISBN 9781118704417. doi: 10.1002/9781118704417.ch21. ISBN: 9781118704417.

J.T. Emmert. Thermospheric mass density: A review. *Advances in Space Research*, 56(5):773–824, 2015. ISSN 0273-1177. doi: 10.1016/j.asr.2015.05.038.

D. G. King-Hele and D. W. Scott. Comparison of air densities derived from the orbits of 1966–51A, B and C. In Bruno Morando, editor, *Dynamics of Satellites (1969)*, pages 216–229, Berlin, Heidelberg, 1970. Springer. ISBN 978-3-642-99966-6. doi: 10.1007/978-3-642-99966-6. ISBN: 9783642999666.

S. Bruinsma, D. Tamagnan, and R. Biancale. Atmospheric densities derived from CHAMP/STAR accelerometer observations. *Planetary and Space Science*, 52:297–312, 2004. doi: 10.1016/j.pss.2003.11.004.

Eelco Doornbos. *Thermospheric Density and Wind Determination from Satellite Dynamics*. Springer, Berlin, Heidelberg, 2012. doi: 10.1007/978-3-642-25129-0. ISBN: 9783642251283.

E. K. Sutton, R. S. Nerem, and J. M. Forbes. Density and winds in the thermosphere deduced from accelerometer data. *Journal of Spacecraft and Rockets*, 44(6):1210–1219, 2007. doi: 10.2514/1.28641.

E. K. Sutton. Accelerometer-derived atmospheric densities from the CHAMP and GRACE satellites: Version 2.3. Technical Report ADA537198, Air Force Research Laboratory, NM, USA, February 2011.

Frank E. Grubbs. On estimating precision of measuring instruments and product variability. *Journal of the American Statistical Association*, 43(242):243–264, 1948. doi: 10.2307/2280371.

A. D. Richmond, E. C. Ridley, and R. G. Roble. A thermosphere/ionosphere general circulation model with coupled electrodynamics. *Geophysical Research Letters*, 19(6):601–604, 1992. doi: 10.1029/92GL00401.

T. Kodikara. *Physical Understanding and Forecasting of the Thermospheric Structure and Dynamics*. PhD thesis, RMIT University, Melbourne, Australia, 2019.

Liying Qian, Alan G. Burns, Barbara A. Emery, Benjamin Foster, Gang Lu, Astrid Maute, Arthur D. Richmond, Raymond G. Roble, Stanley C. Solomon, and Wenbin Wang. The NCAR TIE-GCM: A community model of the coupled thermosphere/ionosphere system. In *Modeling the Ionosphere Thermosphere System*, chapter 7, pages 73–83. John Wiley, Washington, 2014. ISBN 9781118704417. doi: 10.1002/9781118704417.ch7. ISBN: 9781118704417.

P. G. Richards, J. A. Fennelly, and D. G. Torr. EUVAC: A solar EUV flux model for aeronomic calculations. *Journal of Geophysical Research: Space Physics*, 99 (A5):8981–8992, 1994. doi: 10.1029/94JA00518.

Stanley C. Solomon and Liying Qian. Solar extreme-ultraviolet irradiance for general circulation models. *Journal of Geophysical Research: Space Physics*, 110(A10), 2005. ISSN 2156-2202. doi: 10.1029/2005JA011160.

K. F. Tapping. The 10.7 cm solar radio flux ($F_{10.7}$). *Space Weather*, 11(7):394–406, 2013. ISSN 1542-7390. doi: 10.1002/swe.20064.

R. A. Heelis, J. K. Lowell, and R. W. Spiro. A model of the high-latitude ionospheric convection pattern. *Journal of Geophysical Research: Space Physics*, 87(A8):6339–6345, 1982. doi: 10.1029/JA087iA08p06339.

R. G. Roble and E. C. Ridley. An auroral model for the NCAR thermospheric general circulation model (TGCM). *Annales Geophysicae, Series A-Upper Atmosphere and Space Sciences*, 5:369–382, 1987.

Barbara Emery, Raymond Roble, E Ridley, Arthur Richmond, Delores Knipp, Geoff Crowley, David Evans, Frederick Rich, and Sawako Maeda. Parameterization of the ion convection and the auroral oval in the ncar thermospheric general circulation models. Technical report, 2012. URL http://opensky.ucar.edu/islandora/object/technotes:501. No. NCAR/TN-491+STR.

M. E. Hagan, R. G. Roble, and J. Hackney. Migrating thermospheric tides. *Journal of Geophysical Research: Space Physics*, 106(A7):12739–12752, 2001. doi: 10.1029/2000JA000344.

Liying Qian, Stanley C. Solomon, and Timothy J. Kane. Seasonal variation of thermospheric density and composition. *Journal of Geophysical Research: Space Physics*, 114(A1), 2009. ISSN 2156-2202. doi: 10.1029/2008JA013643.

J. T. Emmert, D. P. Drob, J. M. Picone, D. E. Siskind, M. Jones Jr., M. G. Mlynczak, P. F. Bernath, X. Chu, E. Doornbos, B. Funke, L. P. Goncharenko, M. E. Hervig, M. J. Schwartz, P. E. Sheese, F. Vargas, B. P. Williams, and T. Yuan. NRLMSIS 2.0: A whole-atmosphere empirical model of temperature and neutral species densities. *Earth and Space Science*, 8(3): e2020EA001321, 2021. doi: 10.1029/2020EA001321.

Jeremiah P. Sjoberg, Richard A. Anthes, and Therese Rieckh. The three-cornered hat method for estimating error variances of three or more atmospheric datasets. part i: Overview and evaluation. *Journal of Atmospheric and Oceanic Technology*, 38(3):555–572, 2021. doi: 10.1175/JTECH-D-19-0217.1.

H. Liu, H. Lühr, V. Henize, and W. Köhler. Global distribution of the thermospheric total mass density derived from CHAMP. *Journal of Geophysical Research: Space Physics*, 110(A4), 2005. doi: 10.1029/2004JA010741.

M. Rother and I. Michaelis. CH-ME-2-PLPT - CHAMP electron density and temperature time series in low time resolution (level 2). *GFZ Data Services*, 2019. doi: 10.5880/GFZ.2.3.2019.007.

D. P. Drob, J. T. Emmert, G. Crowley, J. M. Picone, G. G. Shepherd, W. Skinner, P. Hays, R. J. Niciejewski, M. Larsen, C. Y. She, J. W. Meriwether, G. Hernandez, M. J. Jarvis, D. P. Sipler, C. A. Tepley, M. S. O'Brien, J. R. Bowman, Q. Wu, Y. Murayama, S. Kawamura, I. M. Reid, and R. A. Vincent. An empirical model of the Earth's horizontal wind fields: HWM07. *Journal of Geophysical Research: Space Physics*, 113(A12), 2008. ISSN 2156-2202. doi: 10.1029/2008JA013668.

Matthias Förster and Eelco Doornbos. Upper thermosphere neutral wind cross-track component deduced from CHAMP accelerometer data. *GFZ Data Services*, 2019. doi: 10.5880/GFZ.1.1.2019.001.

P Tavella and A Premoli. Estimating the instabilities ofNClocks by measuring differences of their readings. *Metrologia*, 30(5):479–486, 1994. doi: 10.1088/0026-1394/30/5/003.

Francisco Javier Galindo, Juan José Ruiz, Eleonora Giachino, Amedeo Premoli, and Patrizia Tavella. Estimation of the covariance matrix of individual standards by means of comparison measurements. In *Advanced Mathematical and Computational Tools in Metrology V*, volume 57, chapter 20, pages 177–184. World Scientific, Singapore, 2001. ISBN 9789810244941. doi: 10.1142/9789812811684_0020. ISBN: 9789810244941.

Travis Lechtenberg, Craig A. McLaughlin, Travis Locke, and Dhaval Mysore Krishna. Thermospheric density variations: Observability using precision satellite orbits and effects on orbit propagation. *Space Weather*, 11(1): 34–45, 2013. doi: 10.1029/2012SW000848.